Anomalous neuronal responses to fluctuated inputs

Ryosuke Hosaka[*]
Department of Applied Mathematics, Fukuoka University, Fukuoka Prefecture 814-0180, Japan

Yutaka Sakai[†]
Tamagawa University Brain Science Institute, Tokyo 194-8610, Japan

(Received 14 May 2015; revised manuscript received 15 September 2015; published 7 October 2015)

The irregular firing of a cortical neuron is thought to result from a highly fluctuating drive that is generated by the balance of excitatory and inhibitory synaptic inputs. A previous study reported anomalous responses of the Hodgkin-Huxley neuron to the fluctuated inputs where an irregularity of spike trains is inversely proportional to an input irregularity. In the current study, we investigated the origin of these anomalous responses with the Hindmarsh-Rose neuron model, map-based models, and a simple mixture of interspike interval distributions. First, we specified the parameter regions for the bifurcations in the Hindmarsh-Rose model, and we confirmed that the model reproduced the anomalous responses in the dynamics of the saddle-node and subcritical Hopf bifurcations. For both bifurcations, the Hindmarsh-Rose model shows bistability in the resting state and the repetitive firing state, which indicated that the bistability was the origin of the anomalous input-output relationship. Similarly, the map-based model that contained bistability reproduced the anomalous responses, while the model without bistability did not. These results were supported by additional findings that the anomalous responses were reproduced by mimicking the bistable firing with a mixture of two different interspike interval distributions. Decorrelation of spike trains is important for neural information processing. For such spike train decorrelation, irregular firing is key. Our results indicated that irregular firing can emerge from fluctuating drives, even weak ones, under conditions involving bistability. The anomalous responses, therefore, contribute to efficient processing in the brain.

DOI: 10.1103/PhysRevE.92.042705 PACS number(s): 87.19.ll, 87.85.dm

I. INTRODUCTION

Cortical neurons generate irregular spike trains, including highly variable intervals [1–3]. Irregular spiking has received much attention because it plays functionally important roles in neural information processing [4–7]. The origins of these irregularities are intrinsic noise, such as synaptic unreliability [8] and ion-channel noise [9], and highly fluctuating drives that are generated by the balance of the excitatory and inhibitory synaptic inputs to the neurons [10–15]. Neuronal responses have traditionally been characterized by their frequency-current relationship [16,17]. However, the frequency-current relationship is not sufficient for understanding the neuronal responses to fluctuated inputs. Several studies have described the responses of neurons to fluctuated inputs, and reactive differences have been reported among neuron models [15,18–25].

Regarding the response to the fluctuated inputs, an interesting phenomenon has been reported [26]: "The variability of output spike trains of the Hodgkin-Huxley (HH) neuron model decreases as the input variance increases." This inverse relationship between input and output variances is seemingly counterintuitive. Thus, we call it an anomalous response. A schematic representation of an anomalous response is shown in Fig. 1. Sakai *et al.* suggested that the underlying mechanism of the anomalous responses of HH neurons may originate from the subthreshold oscillations of the membrane potential. In fact, the input-output (I-O) relationship of a leaky integrate-and-fire (LIF) neuron model, which does not contain subthreshold oscillations, is proportional [Fig. 1(b)]. A similar phenomenon has also been observed in an experimental study [27].

Although their findings were important and fundamental, further analyses are required because the comparison was performed with models with dynamics that were very different from each other. The HH and LIF models differ in a number of ways, including the complexity of their dynamics, the number of variables, and the number of parameters. Moreover, the HH model is too complicated to use to determine the origin of the anomalous responses. Therefore, we have been unable to verify that subthreshold oscillations are the origin of the anomalous responses as Sakai *et al.* concluded. In addition, other components may cause or contribute to the anomalous responses. Thus, the purpose of this study was to reveal the origin of the anomalous responses.

The two major differences between the HH and LIF models are the subthreshold oscillations of the membrane potential and the bistability of the attractors (resting and repetitive firing). The HH model has both, while the LIF model has neither. To examine the origins of the anomalous responses, a neuron model that can separate the subthreshold oscillations and the bistability should be used. One plausible choice is the Morris-Lecar model, which consists of three coupled differential equations that incorporate only two essential ionic currents, namely the potassium current and the calcium current [28]. Although this model contains both subthreshold oscillations and bistability, it is not appropriate because it requires large parameter alterations to switch behaviors. In the current study, we employed the Hindmarsh-Rose (HR) neuron model [29]. The HR model is a neuron model that is described by only two variables, and it has fewer parameters than the HH model. The HR model exhibits both subthreshold oscillations and bistability by controlling only two parameters.

[*]hosaka@fukuoka-u.ac.jp
[†]sakai@tamagawa.ac.jp

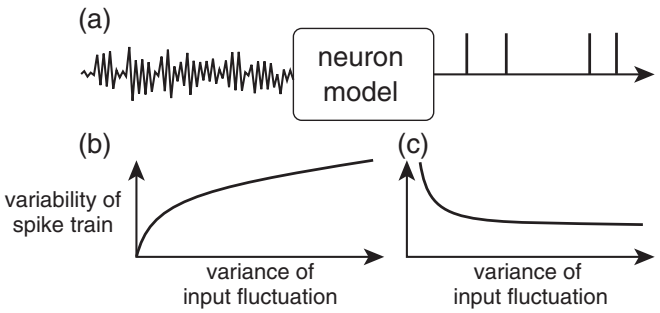

FIG. 1. Schematic representation of the anomalous responses in the Hodgkin-Huxley neuron model [26]. (a) The neuron model receives the uncorrelated fluctuation that mimics the balancing of synaptic inputs and generates an output spike train. (b) The variability of the spike train is shown as a function of the variance of the input fluctuation. For a leaky integrate-and-fire neuron model, the variability of the spike train increases as the input variance increases. (c) For the Hodgkin-Huxley neuron model, the variability of the spike train decreases as the input variance increases.

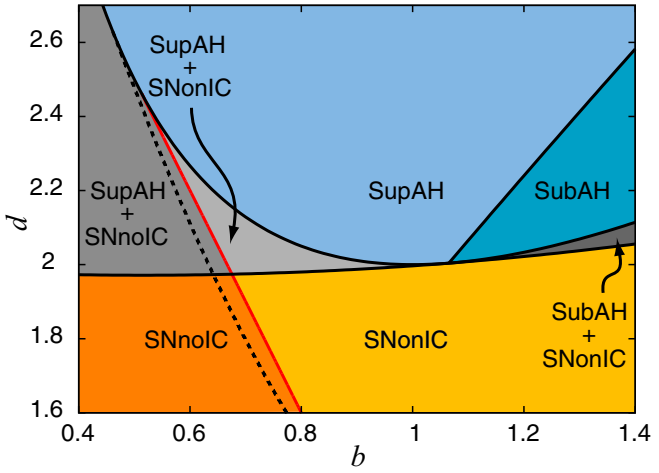

FIG. 2. (Color online) Parameter regions of the Hindmarsh-Rose (HR) model of the bifurcations. The solid black lines indicate the boundaries between the bifurcations. The dashed black line indicates the boundary between the saddle node on the invariant circle (SNonIC) and the saddle node not on the invariant circle (SNnoIC) bifurcations when the time constant of the membrane potential τ is $3^2/b$. The solid red line indicates the boundary when τ tends to positive infinity (see Appendix A).

First, we demonstrated that the HR model separated the subthreshold oscillations and bistability and that the origin of the anomalous responses was the bistability and not the subthreshold oscillations. We then found that the same results were obtained with map-based models. A map-based model that contained bistability reproduced the anomalous responses, while the map-based model that did not contain bistability did not. These results were further supported by the findings that the anomalous responses were reproduced by a simple mixture of two interspike interval (ISI) distributions.

II. METHODS

A. The Hindmarsh-Rose model

The HR model is described as follows:

$$\dot{x} = x - x^3/3 - y + I(t), \quad (1)$$
$$\tau \dot{y} = (x^2 + dx + a)/b - y, \quad (2)$$

where $\dot{x}$ represents a temporal derivative of x, and τ corresponds to a membrane time constant. Unless otherwise stated, $3^2/b$ was the value of τ. When x exceeds a threshold of 0.5, the neuron generates an action potential. $I(t)$ describes an external input that is applied to the model (Sec. II C). One of the fixed points in the HR model mimics the resting potential. The fixed point becomes unstable through one of the following four types of bifurcation forms: saddle-node bifurcation on the invariant circle (SNonIC), saddle-node bifurcation not on the invariant circle (SNnoIC), supercritical Andronov-Hopf bifurcation (SupAH), and subcritical Andronov-Hopf bifurcation (SubAH) [30]. These four bifurcations correspond to different combinations of the subthreshold oscillations and bistabilities. The correspondence is summarized in Table I [31]. The HR model can exhibit the four bifurcations by operating the two parameters (b,d) [29,30]. The parameter region for each bifurcation is depicted in Fig. 2. We provide the derivations of the parameter regions in Appendix A. Note that the HR model exhibits many other bifurcations in addition to the above four bifurcations [30]. The following (b,d) values were used as the typical parameter values for each bifurcation: (1.0,1.8) for the SNonIC bifurcation, (0.6,1.8) for the SNnoIC bifurcation, (1.0,2.2) for the SupAH bifurcation, and (1.3,2.2) for the SubAH bifurcation. To make the bifurcations occur at $I(t) = 0$, parameter a was 0.073 705 for the SNonIC bifurcation, −0.126 226 for the SNnoIC bifurcation, 0.521 833 for the SupAH bifurcation, and 0.319 832 for the SubAH bifurcation. The nullclines and stable attractors are depicted in Fig. 3. The stable fixed point of the SNnoIC bifurcation was located outside the stable limit cycle, whereas that of the SubAH bifurcation was located inside the stable limit cycle. The current-frequency relationships are provided in Fig. 4.

TABLE I. The four types of behaviors and their corresponding bifurcations.

	Subthreshold oscillation	
	no	yes
Monostable	Saddle-node on invariant circle (SNonIC)	Supercritical Andronov-Hopf (SupAH)
Bistable	Saddle-node not on invariant circle (SNnoIC)	Subcritical Andronov-Hopf (SubAH)

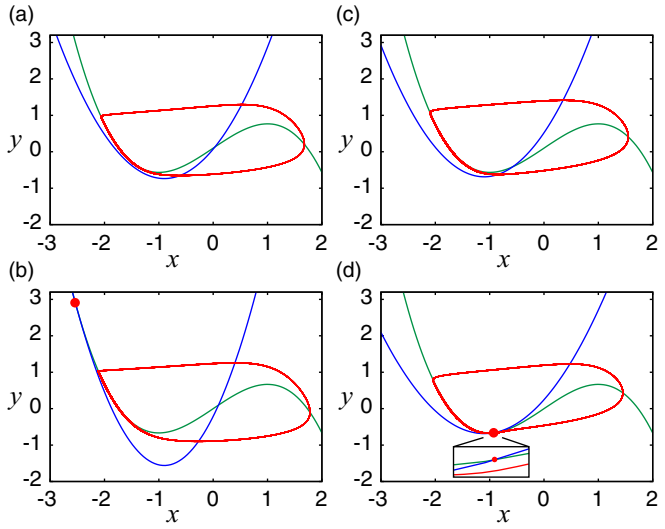

FIG. 3. (Color online) Nullclines and stable attractors of the HR model with (a) SNonIC, (b) SNnoIC, (c) supercritical Andronov-Hopf (SupAH), and (d) subcritical Andronov-Hopf (SubAH) bifurcations. The green and blue curves are the x-nullcline and y-nullcline, respectively. The red lines are the stable limit cycle. The red closed circles in (b) and (d) are the stable fixed points. Parameter I is 0.1 for the SNonIC and SupAH bifurcations and 0 for the SNnoIC and SubAH bifurcations.

B. The map-based models

1. The subcritical Rulkov model

The discrete-time dynamical systems that are valid phenomenological models of neurons are known as map-based models [32]. The Rulkov model is a map-based model that replicates spiking-bursting neural activity [33]. The bifurcation of the fixed point in this model is the SubAH bifurcation [34]. This model is therefore capable of containing bistability [32]. We will refer to this model as the subcritical Rulkov model for clarity. The subcritical Rulkov model is described as follows:

$$x_{n+1} = F_{\text{sub}}(x_n, y_n), \tag{3}$$

$$y_{n+1} = y_n + (-x_n + s + I_n)/\tau, \tag{4}$$

where x_n is the fast and y_n is the slow dynamical variable. The slow time evolution of y_n is due to the large value of the parameter τ, and $\tau = 100$ in this study. I_n describes an external input that is applied to the model (Sec. II C). s is the control parameter that is used to select the regimen of individual behavior, and s was set to $1 - \sqrt{\frac{\alpha}{1-1/\tau}}$ in order to make the bifurcation occur at $I_n = 0$. The subcritical Rulkov model uses $s' = s + 1$ in its original formulation [33]. $F_{\text{sub}}(x, y)$ is a function that represents the subthreshold behavior of the membrane potential, and it includes a threshold and reset mechanism to produce spikes:

$$F_{\text{sub}}(x,y) = \begin{cases} \frac{\alpha}{(1-x)} + y & \text{if } x \leqslant 0, \\ \alpha + y & \text{if } 0 < x < \alpha + y, \\ -1 & \text{if } x \geqslant \alpha + y, \end{cases}$$

where $\alpha = 4$ in this study.

2. The supercritical Rulkov model

For the map-based model that did not exhibit bistability, the model that was proposed by Shilnikov and Rulkov was employed [35]. We refer to this map-based model as the supercritical Rulkov model because the bifurcation of the fixed point in this model is the SupAH bifurcation [35]. This model is described as follows:

$$x_{n+1} = F_{\text{sup}}(x_n, y_n), \tag{5}$$

$$y_{n+1} = y_n + (-x_n + s + I_n)/\tau, \tag{6}$$

where

$$F_{\text{sup}}(x,y) = \begin{cases} \frac{-\alpha^2}{4} - \alpha + y & \text{if } x < -1 - \alpha/2, \\ \alpha x + (x+1)^2 + y & \text{if } -1 - \alpha/2 \leqslant x \leqslant 0, \\ 1 + y & \text{if } 0 < x < 1 + y, \\ -1 & \text{if } x \geqslant 1 + y, \end{cases}$$

where $\tau = 100$ and $\alpha = 1$ in this study. s was set to $-\{1 + 1/\tau + \alpha\}/2$ to make the bifurcation occur at $I_n = 0$. I_n describes an external input that is applied to the model (Sec. II C). This model exhibits a small-amplitude subthreshold oscillation, which is the same as the HR model with the SupAH bifurcation.

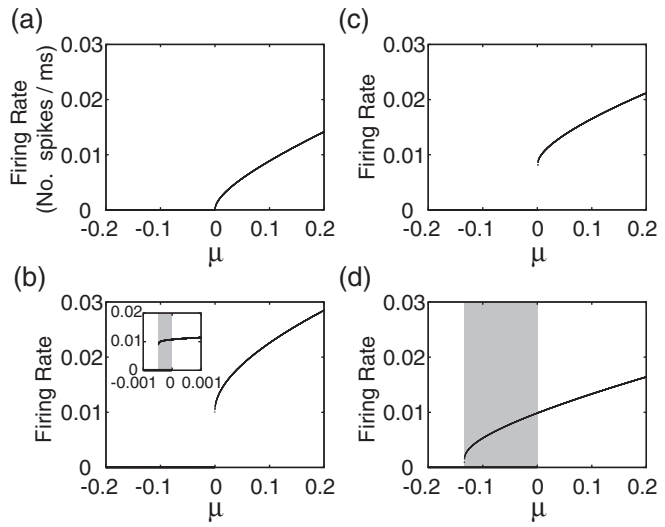

FIG. 4. Frequency-current relationship of the HR model with (a) SNonIC, (b) SNnoIC, (c) SupAH, and (d) SubAH bifurcations. The input is a constant current, $I(t) = \mu$. The gray regions in (b) and (d) indicate the bistable conditions.

C. Input fluctuation

The inward current to a cell body, $I(t)$ in Eq. (1) and I_n in Eqs. (4) and (6), is described by the form

$$I(t) = \mu + \sigma\xi(t),$$

$$I_n = \mu + \sigma\xi_n,$$

where $\xi(t)$ and ξ_n are white Gaussian noise. The parameters μ and σ control the mean and fluctuation of the inputs,

respectively. This fluctuated input was based on the following assumption: a cortical neuron receives thousands of synaptic contacts; if the incoming synaptic inputs are assumed to be independent, then the sum of a large number of independent excitatory and inhibitory inputs can be approximated to an uncorrelated fluctuation [36].

D. Interspike interval statistics

The output spike trains were evaluated with two ISI statistics: the mean ISI ($\overline{T}$) and the coefficient of variation (C_v), which were defined as

$$\overline{T} = \frac{1}{n}\sum_{i=1}^{n} T_i,$$

$$C_v = \sqrt{\overline{(T_i - \overline{T})^2}}/\overline{T},$$

where T_i represents the ISI. C_v evaluates the irregularity of the spike trains. If the spike train is completely regular, that is, if all of the ISIs are constant, then C_v corresponds to 0. If the spike train is completely random, which indicates a Poisson process, then C_v corresponds to 1. Because C_v is a dimensionless quantity, we can directly compare C_v in the various models. In contrast, $\overline{T}$ is not a dimensionless value. We therefore used the ratio of $\overline{T}$ to the membrane time constant, $\overline{T}/\tau$, for comparison. We estimated ($\overline{T}/\tau$, C_v) from a finite ISI sequence consisting of 10 000 ISIs that were obtained with a numerical simulation.

E. The Markov transition bistability model

As a simple model of bistability, a mixture of two types of ISIs was introduced. In the repetitive firing state, the neuron emits spikes at a constant ISI. In the resting state, the spikes occur accidentally due to the large fluctuations of the external inputs, which result in variable ISIs. Thus, a mixture of constant ISIs and variable ISIs was used. Although this ISI mixture can be described in several ways, one plausible option is the introduction of a Markov switching mechanism. Namely, the ISIs were produced randomly with a Markov process of current mode switching between the constant mode and the variable mode [Fig. 9(a)].

In the constant mode, every ISI was equal to the constant value r: spikes occurred regularly at a constant interval r. In the variable mode, every ISI was produced randomly through the sampling of the distributions $F_0(T)$. The next mode was chosen independently with a probability p for the variable mode and $1-p$ for the constant mode. In the mixture of constant ISIs and variable ISIs, F_p is expressed with F_0 and p as follows:

$$F_p(T) = (1-p)\delta(T-r) + pF_0(T),$$

where δ is the Dirac delta function and T is an ISI. The statistical quantity ($\overline{T}$,C_v) is easily obtained from the moments of the ISI distribution $F_0(T)$ (Appendix B).

We assumed three distributions for $F_0(T)$: the exponential distribution,

$$F_e(T|\lambda) = \lambda e^{-\lambda T}; \tag{7}$$

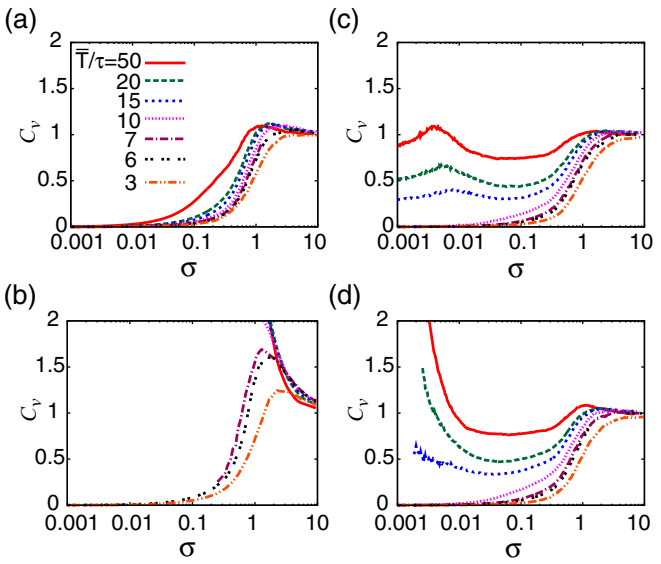

FIG. 5. (Color online) Relationship between input variance σ and output variance C_v for the HR model with (a) SNonIC, (b) SNnoIC, (c) SupAH, and (d) SubAH bifurcations.

the exponential distribution with an absolute refractory period R,

$$F_R(T|\lambda,R) = \lambda e^{-\lambda T} + R; \tag{8}$$

and the Γ distribution,

$$F_\gamma(T|\lambda,\alpha) = \frac{\lambda^\alpha}{\Gamma(\alpha)} e^{-\lambda T} T^{\alpha-1}, \tag{9}$$

where $\Gamma(\alpha)$ is the Gamma function. We set the constant ISI to $r = 2.5\tau$. Changing the input parameter values (μ,σ) corresponded to changing λ and p in this model.

III. RESULTS

A. The Hindmarsh-Rose model

1. *The HR model with the SubAH bifurcation reproduced the anomalous responses*

We first investigated whether the HR model reproduced the anomalous I-O relationship that was observed with the HH model. Figure 5 shows the dependence of C_v on the input variance σ under each bifurcation condition, where the input mean μ was altered so that $\overline{T}/\tau$ was constant.

The HR model with the SNonIC bifurcation did not exhibit subthreshold oscillations or bistability (Table I), which was similar to the LIF model. C_v of this model increased as σ increased [Fig. 5(a)], which indicated that the irregularity of the output spike trains was proportional to the magnitude of the input fluctuations. This was true regardless of the $\overline{T}/\tau$ value. A similar orbit of C_v was observed in the LIF model [26].

The HR model with the SubAH bifurcation exhibited both subthreshold oscillations and bistability (Table I), which was similar to the HH model. As shown in Fig. 5(d), when $\overline{T}/\tau \leqslant 10$, C_v of this model was proportional to σ, and it resembled that of the SNonIC bifurcation.

When $\overline{T}/\tau > 20$, C_v took on a different appearance: C_v was inversely proportional to σ, especially when $0.001 < \sigma < 0.1$.

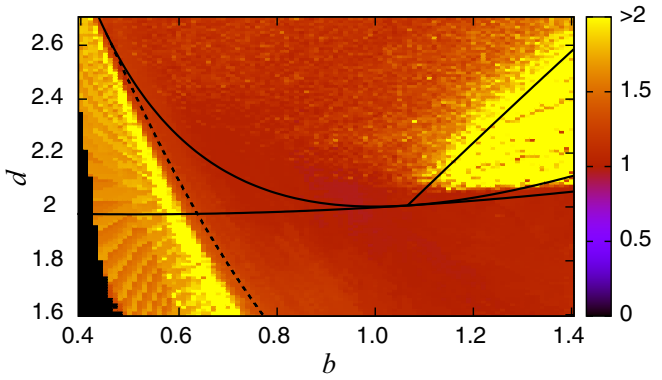

FIG. 6. (Color online) The largest C_v value for the spike trains with $\overline{T}/\tau = 50$ for each parameter (b, d). The solid and dashed lines are the boundary between the bifurcations, as in Fig. 2.

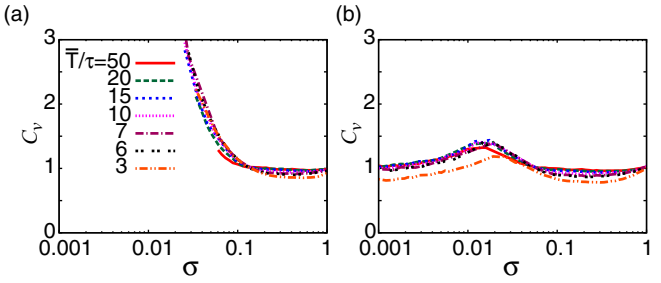

FIG. 7. (Color online) Relationship between input variance σ and output variance C_v for the map-based models: (a) the subcritical Rulkov model and (b) the supercritical Rulkov model.

When $\overline{T}/\tau = 50$, C_v exceeded 1 for $\sigma < 0.01$, and it decreased as σ increased. This inverse relationship was similar to that observed in the HH model [26], which suggested that the HR model was sufficiently complex to reproduce the anomalous responses and that the subthreshold oscillations and bistability were candidates for the origin of the anomalous responses.

2. *The origin of the anomalous responses: Subthreshold oscillations or bistability*

To clarify the origin of the anomalous responses, the subthreshold oscillations, or bistability, we calculated C_v values for the HR model with the SupAH bifurcation and the HR model with the SNnoIC bifurcation. The HR model with the SupAH bifurcation showed subthreshold oscillations but no bistability (Table I). In contrast, the HR model with the SNnoIC bifurcation showed bistability but no subthreshold oscillations (Table I).

Figure 5(c) depicts C_v values of the HR model with the SupAH bifurcation. The orbits of C_v on $\overline{T}/\tau \leqslant 10$ were similar to those of the SubAH bifurcation [Fig. 5(d)]. However, the orbits of C_v on $\overline{T}/\tau \geqslant 15$ differed from those of the SubAH bifurcation: below $\sigma \leqslant 0.1$, C_v remained constant even as σ increased. These results indicated that the subthreshold oscillations were not an origin of the anomalous responses.

Figure 5(b) depicts C_v values of the HR model with the SNnoIC bifurcation. When $\overline{T}/\tau \geqslant 20$, C_v was larger than 2 for $\sigma < 2$. As σ increased, C_v declined and converged to 1, which indicated that the bistability might be the origin of the anomalous responses. C_v of $\overline{T}/\tau = 3$ was proportional to σ. C_v of $\overline{T}/\tau = 6$ and 7 showed intermediate behavior between the anomalous responses and proportional relationships: C_v was almost 0 for small σ, and it increased as σ increased until σ reached 1; C_v then began to decrease and finally converged to 1.

To evaluate the anomalous responses in the entire parameter space, the largest C_v value for the spike trains with $\overline{T}/\tau = 50$ was calculated by sweeping the (b, d) parameter space (Fig. 6). For the anomalous responses, the largest C_v value should be larger than 1, and it is typically larger than 2. Otherwise, the largest C_v should be lower than 2. The largest value of C_v exceeded 2 with the parameters of the SubAH (right upper region of Fig. 6) and SNnoIC (left region of Fig. 6) bifurcations. Based on these results, the bistability of the resting states and repetitive firing, and not the subthreshold oscillations, was determined to be the origin of the anomalous responses.

B. The map-based models

If the anomalous responses depended only on the bistability, the same could be predicted for the map-based neuron models. The subcritical Rulkov model shows bistability with the appropriate parameters (Sec. II B 1) [33]. The ISI statistics of the subcritical Rulkov model were calculated [Fig. 7(a)]. The subcritical Rulkov model reproduced the anomalous responses regardless of the value of $\overline{T}/\tau$: C_v was larger than 2 for $\sigma < 0.04$; as σ increased, C_v declined and converged to 1.

To investigate if the map-based model without bistability failed to reproduce the anomalous responses, the ISI statistics of the supercritical Rulkov model were calculated [Sec. II B 2, Fig. 7(b)]. The supercritical Rulkov model did not reproduce the anomalous responses: regardless of the value of $\overline{T}/\tau$, C_v was almost constant, and it ranged between 1 and 1.5 for any value of σ.

C. Spike trains with large C_v values

To clarify how the bistability produces the highly irregular spike trains, the spike trains of the map-based models are depicted in Fig. 8. For the subcritical Rulkov model, spike trains with large C_v values ($C_v = 2$) contained burstlike spikes, which were a successive occurrence of spikes [Fig. 8(a), enlargement]. The mean ISI of this spike train was small due to the burstlike spikes, while the variance of the ISIs was large due to a composite of short ISIs inside the burst and long ISIs outside the burst. Therefore, the large C_v values were realized by the burstlike spikes that were formed by the bistability. As σ increased, the number of spikes that were included in a single burst gradually decreased, and the spike train settled eventually into a Poisson spike train [Fig. 8(b), $C_v = 1$].

The burstlike spike train did not emerge in the supercritical Rulkov model. Only small clusters of spikes were included in the spike trains with the largest C_v values [Fig. 8(c), $C_v = 1.4$]. As σ decreased, the probability of the occurrence of the clusters of spikes decreased. For small σ, the spikes were more likely to occur at the top of the subthreshold oscillations [Fig. 8(d), enlargement]. The probability of spike

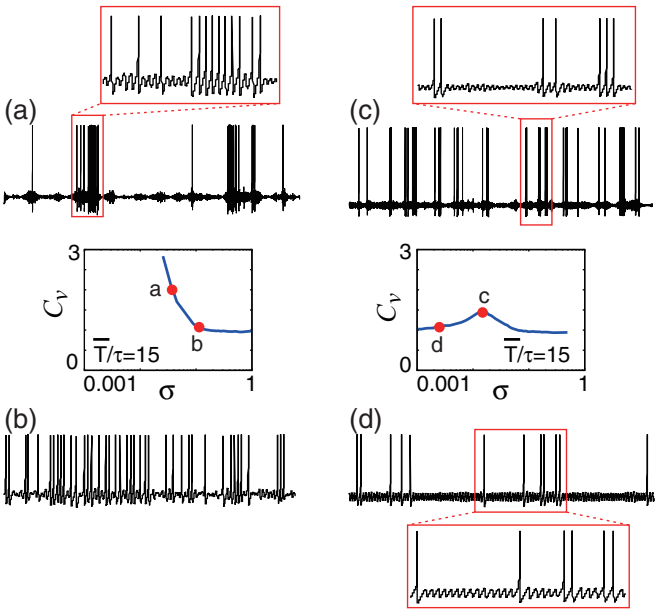

FIG. 8. (Color online) Example spike trains of (a),(b) the subcritical and (c),(d) supercritical Rulkov models in which $\overline{T}/\tau = 15$. The middle panels ($\sigma - C_v$ planes) indicate (σ, C_v) of each example spike train. (a) The spike train of $C_v = 2$. An enlargement of one of the burstlike spikes is depicted in the upper red box. (b) The spike train with $C_v = 1$. (c) The spike train with $C_v = 1.4$. Three of the clustering spikes are enlarged in the upper red box. (d) The spike train with $C_v = 1$. An enlargement in the lower red box shows the spikes being phase-locked to the top of the subthreshold oscillation.

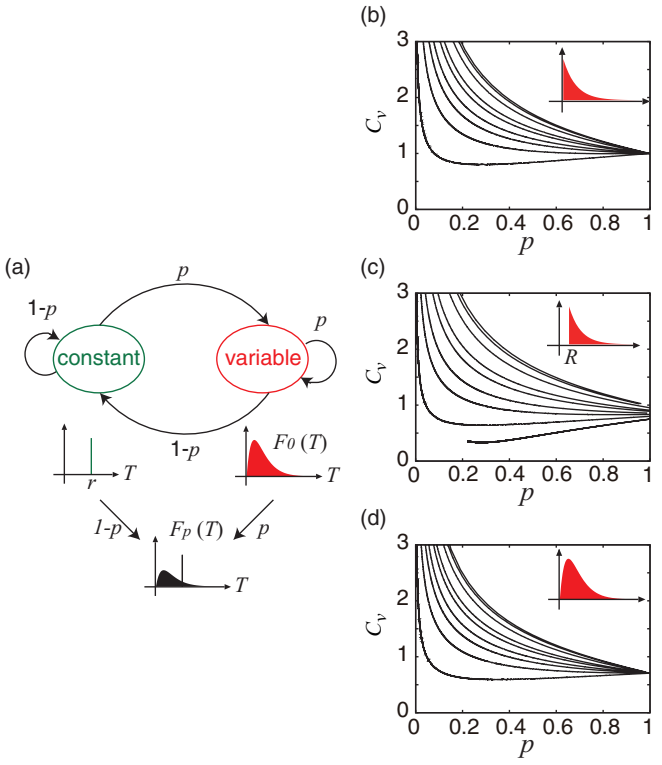

FIG. 9. (Color online) The Markov transition bistability model. (a) Schematic of the mixture of constant interspike intervals (ISIs) and variable ISIs. The ISI mixture can be produced with a Markov switching mechanism. The spiking mode switches between the constant and variable ISI modes with probability p. (b)–(d) The lines indicate C_v contours with $\overline{T}/\tau = 3$, 4, 5, 6, 8, 10, 20, 50, and 100 from bottom to top, respectively. The inset shows the distribution that was used for the variable ISIs.

generation was stochastic due to the input fluctuation. This spike train corresponded to a discrete Poisson spike train, in which $C_v = 1$.

D. The Markov transition bistability model

1. Heterogeneous ISI distributions

To confirm the above findings in a more simplified model, we examined a simple mixture of the two types of ISIs. Namely, the ISIs were produced randomly with current mode switching between the constant mode and the variable mode in a Markov process [Fig. 9(a)]. This is one of the simplest models of bistable firing.

We first considered a case in which the spike times followed a Poisson process in the variable mode. In this case, the ISIs exhibited an exponential distribution, Eq. (7). We obtained $(\overline{T}, C_v)$ with $F_e(T|\lambda)$ for the variable ISIs $F_0(T)$. Figure 9(b) depicts the $\overline{T}/\tau$ contour lines in the p-C_v plane that was obtained by sweeping λ of $F_e(T|\lambda)$. The model showed the anomalous responses, regardless of the statistics used for $\overline{T}/\tau$: C_v was large for $p \sim 0$, and it decreased and converged to 1 as p increased.

We then considered a case with spike trains that followed the Poisson process with an absolute refractory period. In this case, the ISIs exhibited an exponential distribution with a positive temporal shift due to the refractory period, Eq. (8). The refractory period R was set to τ. Figure 9(c) depicts the $\overline{T}/\tau$ contour lines by sweeping λ of $F_R(T|\lambda, R)$. The model showed the anomalous responses: C_v was large for $p \sim 0$, and it decreased to $\overline{T}/(\overline{T} + R)$ as p increased. C_v of $\overline{T}/\tau = 3$ for $p < 0.2$ could not be obtained because such fast spike trains could not be reproduced with these parameters.

We finally examined more general spike trains in which the ISIs exhibited a Γ distribution, Eq. (9). Figure 9(d) shows the case in which $\alpha = 2$. As in the previous two models, this model showed the anomalous responses: C_v was large for $p \sim 0$, and it decreased to $1/\sqrt{\alpha}$ as p increased. Quantitatively, the same contour lines were obtained for other α values ($\alpha = 3$, 4, 5, and 10; not shown).

2. Homogeneous ISI distributions

The questions of whether the mixture of two types of variable ISIs reproduced the anomalous responses or whether the bistability of the two types of constant ISIs produced the anomalous responses arose. To answer these questions, we first investigated a case in which both modes were variable ISIs [Fig. 10(a), insets]. In this study, both distributions were assumed to be the Γ distributions, $F_{\gamma_1}(T|\lambda_1,\alpha_1)$ and $F_{\gamma_2}(T|\lambda_2,\alpha_2)$. The parameters α_1 and α_2 were set to 2. Figure 10(a) depicts the $\overline{T}/\tau$ contour lines in the p-C_v plane that were obtained by sweeping λ_1, while λ_2 was fixed to $\alpha_2/2.5\tau$. This model reproduced the anomalous responses: C_v decreased as p increased and converged to $1/\sqrt{\alpha_2}$ for $p = 1$.

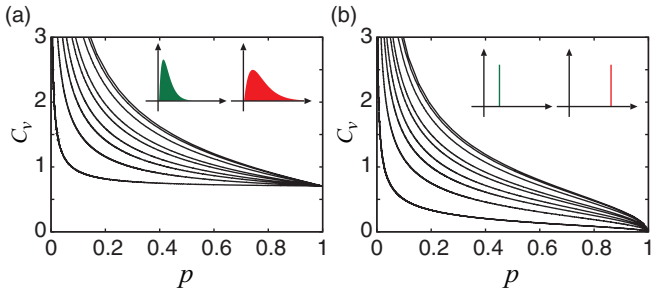

FIG. 10. (Color online) The mixture of (a) two types of variable ISIs and (b) two types of constant ISIs. The insets show the distributions that were used for the two modes. The basic display format is the same as that described in Fig. 9.

We then investigated the case in which both modes were composed of constant ISIs [Fig. 10(b), insets]. Every ISI in one mode was the constant value r_1; every ISI in the other mode was the constant value r_2. Figure 10(b) depicts the $\overline{T}/\tau$ contour lines that were obtained by sweeping r_1, while r_2 was fixed to 2.5τ. This model reproduced the anomalous responses: C_v decreased as p increased and converged to 0 for $p = 1$.

IV. DISCUSSION

We demonstrated that the HR model reproduced anomalous I-O relationships under SNnoIC and SubAH conditions. Under both bifurcations, the HR model exhibited bistability of the resting and repetitive firing states. These results were consistent with the ISI statistics of the map-based models and the simple mixture of the two types of ISI distributions. Therefore, the origin of the anomalous I-O relationship was the bistability of the resting state and the repetitive firing state. Spike correlations in recurrent neural networks are considerably smaller than expected based on the amount of shared presynaptic inputs [37,38], and the decorrelation of the spike trains is important for information processing [39]. Our results indicated that bistability enables the irregular neuronal spike trains, even with small fluctuations of the inputs. Thus, the bistability contributed to efficient neural processing.

The bistability of the resting state and the repetitive firing state has been observed in biological neurons in the entorhinal cortex of the brain [40]. In these neurons, the activity-dependent changes of the Ca^{2+}-sensitive cationic current play a critical role. The entorhinal cortex, which is the main interface between the hippocampus and the cortex, is known as the substrate of conscious memory. The anomalous responses may play some role in memory formation in the entorhinal cortex.

In this study, the bistability of the resting states and the repetitive firing state was realized with an intrinsic bifurcation mechanism in the models. However, bistability can be realized based on the Up/Down states of the membrane potential [41]. The Up/Down states consist of two distinct levels of membrane potentials of neurons. In cortical neurons, the membrane potential stays around −65 mV in Down states and −45 mV in Up states. The firing probability in the Up state is much higher than that in the Down state. Cortical neurons often exhibit spontaneous transitions between the Up and Down states. The Up/Down states can be considered the bistability of attractors. The anomalous responses due to the Up/Down states may be observed in the whole neocortex.

C_v values of the HR model with the SNnoIC and SubAH bifurcations showed different orbits, despite both bifurcations containing bistability (Fig. 5). The relative positions of the stable fixed point are different between the two bifurcations: the stable fixed point of the SNnoIC bifurcation is located outside the stable limit cycle, whereas that of the SubAH bifurcation is located inside the limit cycle (Fig. 3). For the SubAH bifurcation, even small fluctuations of input can prompt the transition between two attractors. However, for the SNnoIC bifurcation, a large fluctuation is required to transit between two attractors. This would therefore cause the different orbits of C_v for the SNnoIC and SubAH bifurcations.

ACKNOWLEDGMENT

We thank Dr. S. Tsuji for valuable discussions.

APPENDIX A: BIFURCATION CONDITIONS

1. Condition for the Andronov-Hopf bifurcation

A Jacobian matrix around fixed point x_0 is $\begin{pmatrix} 1-x_0^2 & -1 \\ (2x_0+d)/b\tau & -1/\tau \end{pmatrix}$, and its eigenequation becomes $\lambda^2 + \lambda\{1/\tau + x_0^2 - 1\} + (bx_0^2 - b + 2x_0 + d)/b\tau = 0$. Since eigenvalues of the Andronov-Hopf bifurcation point are complex conjugates, $1/\tau + x_0^2 - 1 = 0$ and $(bx_0^2 - b + 2x_0 + d)/b\tau > 0$. From them and $b\tau = 3^2 > 0$, the condition for the Andronov-Hopf bifurcation is

$$\begin{aligned} x_0 &= \pm\sqrt{1 - 1/\tau}, \\ d &> -bx_0^2 - 2x_0 + b. \end{aligned} \tag{A1}$$

We set $x_0 < 0$ in this study.

2. Boundary between SupAH and SubAH

Let $f(x) := x - x^3/3$ and $g(x) := (x^2 + dx + a)/b$. A criterion to distinguish SupAH and SubAH is given by $D := \{g'(x_0) - 1/\tau\}f'''(x_0) - f''(x_0)\{g''(x_0) - f''(x_0)\}$, $D > 0$ for SupAH and $D < 0$ for SubAH [42]. Thus, $D = 0$ gives a boundary between SupAH and SubAH:

$$d = b/\tau + 2bx_0^2.$$

3. Condition for the saddle-node bifurcation

Since the fixed point $(x_0, f(x_0))$ corresponds to the crossing point of $f(x)$ and $g(x)$, x_0 satisfies

$$x_0 - x_0^3/3 = \left(x_0^2 + dx_0 + a\right)/b. \tag{A2}$$

For the saddle-node bifurcation, Eq. (A2) has one independent root and one multiple root, indicating that Eq. (A2) has two independent inflection points. The inflection points are solutions of first-order derivative of Eq. (A2),

$$bx_0^2 + 2x_0 + d - b = 0, \tag{A3}$$

and its solutions are $x_0 = \{-1 \pm \sqrt{1 - b(d-b)}\}/b$. Equation (A3) must not have a multiple root, resulting in $1 - b(d - b) > 0$. This gives a condition for the saddle-node bifurcation:

$$d < 1/b + b.$$

4. Boundary between SNonIC and SNnoIC

For $\tau \to \infty$, we can analytically calculate the boundary between SNonIC and SNnoIC (the red line in Fig. 2). Given the extremal values of $f(x)$ as $(x_{\mathrm{fex1}}, f(x_{\mathrm{fex1}}))$ and $(x_{\mathrm{fex2}}, f(x_{\mathrm{fex2}}))$, where $f(x_{\mathrm{fex1}}) < f(x_{\mathrm{fex2}})$, the boundary satisfies

$$f(x_{\mathrm{SN}}) = f(x_{\mathrm{fex2}}),$$

where $(x_{\mathrm{SN}}, f(x_{\mathrm{SN}}))$ is the saddle-node bifurcation point. In this case, $x_{\mathrm{SN}} = \{-1 - \sqrt{1 - b(d-b)}\}/b$ and $f(x_{\mathrm{fex2}}) = 2/3$.

Otherwise, the following numerical procedure gives a rough boundary (the dashed line in Fig. 2 for $\tau = 3^2/b$). Given that a limit cycle and its reunion point to $f(x)$ $(x_{\mathrm{re}}, f(x_{\mathrm{re}}))$, the boundary satisfies

$$f(x_{\mathrm{SN}}) = f(x_{\mathrm{re}}).$$

APPENDIX B: $\overline{T}$ AND C_v OF THE MARKOV SWITCHING MODEL

By using first and second cumulants, ψ_1 and ψ_2, respectively, $\overline{T}$ and C_v are calculated as follows:

$$\overline{T} = \psi_1,$$
$$C_v = \sqrt{\psi_2}/\psi_1.$$

These cumulants are obtained from the first and second moments, ϕ_1 and ϕ_2, respectively, as $\psi_1 = \phi_1$, $\psi_2 = \phi_2 - \phi_1^2$. The first and second moments of the Mixture model are calculated as follows:

$$\phi_1 = (1-p)\phi_{c1} + p\phi_{v1},$$
$$\phi_2 = (1-p)\phi_{c2} + p\phi_{v2},$$

where $\phi_{c1} = r$ and $\phi_{c2} = r^2$ are moments of the constant ISI, ϕ_{v1} and ϕ_{v2} are moments of the variable ISIs, and p is the transition probability. For the Γ distribution, $\phi_{v1} = \alpha/\lambda$ and $\phi_{v2} = \alpha(\alpha+1)/\lambda^2$.

[1] W. R. Softky and C. Koch, J. Neurosci. **13**, 334 (1993).
[2] G. R. Holt, W. R. Softky, C. Koch, and R. J. Douglas, J. Neurophysiol. **75**, 1806 (1996).
[3] S. Shinomoto, Y. Sakai, and S. Funahashi, Neural Comput. **11**, 935 (1999).
[4] G. B. Ermentrout, R. F. Galán, and N. N. Urban, Trends Neurosci. **31**, 428 (2008).
[5] A. A. Faisal, L. P. J. Selen, and D. M. Wolpert, Nat. Rev. Neurosci. **9**, 292 (2008).
[6] P. Hänggi, Chem. Phys. Chem. **3**, 285 (2002).
[7] B. Lindner, Phys. Rep. **392**, 321 (2004).
[8] T. Branco and K. Staras, Nat. Rev. Neurosci. **10**, 373 (2009).
[9] J. A. White, J. T. Rubinstein, and A. R. Kay, Trends Neurosci. **23**, 131 (2000).
[10] M. N. Shadlen and W. T. Newsome, Curr. Opin. Neurobiol. **4**, 569 (1994).
[11] M. V. Tsodyks and T. Sejnowski, Network Comput. Neural Syst. **6**, 111 (1995).
[12] C. van Vreeswijk and H. Sompolinsky, Science **274**, 1724 (1996).
[13] D. J. Amit and N. Brunel, Cereb. Cortex **7**, 237 (1997).
[14] Y. Shu, A. Hasenstaub, and D. A. McCormick, Nature (London) **423**, 288 (2003).
[15] S. Ostojic, J. Neurophysiol. **106**, 361 (2011).
[16] D. A. McCormick, B. W. Connors, J. W. Lighthall, and D. A. Prince, J. Neurophysiol. **54**, 782 (1985).
[17] R. K. Powers and M. D. Binder, Rev. Physiol. Biochem. Pharmacol. **143**, 137 (2001).
[18] D. Brown, J. Feng, and S. Feerick, Phys. Rev. Lett. **82**, 4731 (1999).
[19] R. Hosaka, Y. Sakai, and T. Ikeguchi, J. Phys. Soc. Jpn. **75**, 124007 (2006).
[20] N. Fourcaud-Trocmé, D. Hansel, C. van Vreeswijk, and N. Brunel, J. Neurosci. **23**, 11628 (2003).
[21] S. Shinomoto and Y. Tsubo, Phys. Rev. E **64**, 041910 (2001).
[22] S. Schreiber, L. Samengo, and A. V. M. Herz, J. Neurophysiol. **101**, 2239 (2009).
[23] A. N. Burkitt, Biol. Cybern. **95**, 1 (2006).
[24] A. N. Burkitt, Biol. Cybern. **95**, 97 (2006).
[25] F. Müller-Hansen, F. Droste, and B. Lindner, Phys. Rev. E **91**, 022718 (2015).
[26] Y. Sakai, M. Yamada, and S. Yoshizawa, Proc. Int. Joint Conf. Neural Netw. **2**, 1655 (2002).
[27] T. Tateno, A. Harsch, and H. P. C. Robinson, J. Neurophysiol. **92**, 2283 (2004).
[28] C. Morris and H. Lecar, Biophys. J. **35**, 193 (1981).
[29] J. L. Hindmarsh and R. M. Rose, Nature (London) **296**, 162 (1982).
[30] S. Tsuji, T. Ueta, H. Kawakami, H. Fujii, and K. Aihara, Int. J. Bifurcation Chaos Appl. Sci. Eng. **17**, 985 (2007).
[31] E. M. Izhikevich, *Dynamical Systems in Neuroscience: The Geometry of Excitability and Bursting* (MIT Press, Cambridge, MA, 2007).
[32] B. Ibarz, J. M. Casado, and M. A. F. Sanjuan, Phys. Rep. **501**, 1 (2011).
[33] N. F. Rulkov, Phys. Rev. E **65**, 041922 (2002).
[34] A. L. Shilnikov and N. F. Rulkov, Int. J. Bifurcation Chaos Appl. Sci. Eng. **13**, 3325 (2003).
[35] A. L. Shilnikov and N. F. Rulkov, Phys. Lett. A **328**, 177 (2004).
[36] H. C. Tuckwell, *Introduction to Theoretical Neurobiology* (Cambridge University Press, Cambridge, 1988).
[37] E. Zohary, M. Shadlen, and W. Newsome, Nature (London) **370**, 140 (1994).
[38] A. Renart, J. de la Rocha, P. Bartho, L. Hollender, N. Parga, A. Reyes, and K. D. Harris, Science **327**, 587 (2010).
[39] B. Tripp and C. Eliasmith, Cereb. Cortex **17**, 1830 (2007).
[40] A. V. Egorov, B. N. Hamam, E. Fransen, M. E. Hasselmo, and A. A. Alonso, Nature (London) **420**, 173 (2002).
[41] M. Steriade, A. Nunez, and F. Amzica, J. Neurosci. **13**, 3252 (1993).
[42] J. Guckenheimer and P. Holmes, *Nonlinear Oscillations, Dynamical Systems, and Bifurcations of Vector Fields* (Springer-Verlag, New York, 1983).